Spiral wave chimeras in nonlocally coupled bicomponent oscillators

Yang Li, Haihong Li, Yirui Chen, Shun Gao, Qionglin Dai,* and Junzhong Yang
School of Science, Beijing University of Posts and Telecommunications, Beijing 100876, People's Republic of China

(Received 15 August 2023; revised 19 November 2023; accepted 22 November 2023; published 15 December 2023)

Chimera states in nonidentical oscillators have received extensive attention in recent years. Previous studies have demonstrated that chimera states can exist in a ring of nonlocally coupled bicomponent oscillators even in the presence of strong parameter heterogeneity. In this study, we investigate spiral wave chimeras in two-dimensional nonlocally coupled bicomponent oscillators where oscillators are randomly divided into two groups, with identical oscillators in the same group. Using phase oscillators and FitzHugh-Nagumo oscillators as examples, we numerically demonstrate that each group of oscillators supports its own spiral wave chimera and two spiral wave chimeras coexist with each other. We find that there exist three heterogeneity regimes: the synchronous regime at weak heterogeneity, the asynchronous regime at strong heterogeneity, and the transition regime in between. In the synchronous regime, spiral wave chimeras supported by different groups are synchronized with each other by sharing a same rotating frequency and a same incoherent core. In the asynchronous regime, the two spiral wave chimeras rotate at different frequencies and their incoherent cores are far away from each other. These phenomena are also observed in a nonrandom distribution of the two group oscillators and the continuum limit of infinitely many phase oscillators. The transition from synchronous to asynchronous spiral wave chimeras depends on the component oscillators. Specifically, it is a discontinuous transition for phase oscillators but a continuous one for FitzHugh-Nagumo oscillators. We also find that, in the asynchronous regime, increasing heterogeneity leads irregularly meandering spiral wave chimeras to rigidly rotating ones.

DOI: 10.1103/PhysRevE.108.064206

I. INTRODUCTION

Chimera state, a symmetry-breaking spatiotemporal pattern, consists of spatially separated coherent and incoherent behaviors. It was first discovered in nonlocally coupled identical phase oscillators by Kuramoto and Battogtokh in 2002 [1] and later named by Abrams and Strogatz in 2004 [2]. Chimera states have been widely studied in physics, chemistry, biology, and other fields [3–14]. They are not limited to phase oscillators but can also be found in periodic and chaotic maps [15], FitzHugh-Nagumo (FHN) oscillators [16], Ginzburg-Landau oscillators [17–19], Hodgkin-Huxley models [20,21], Hindmarsh-Rose models [22,23], Van der Pol oscillators [24], etc. Meanwhile, in reality, the phenomena of chimera states have been successfully observed in optical [25], chemical [26], and mechanical experiments [27]. Additionally, biological phenomena such as unihemispheric sleep in marine mammals are potentially related to chimera states [28].

Most of the research on chimera states has been focused on one-dimensional systems. However, interesting chimera states have also been discovered in two-dimensional planes [29], torus surfaces [30,31], and three-dimensional spheres [32]. One of the most intriguing types of chimera states is the spiral wave chimeras, where the phase singularity of the normal spiral wave is replaced by an incoherent core. Spiral wave chimeras have been reported numerically in many theoretical models such as phase oscillators [30,33,34], FHN oscillators [35,36], and Rössler oscillators [37], and experimentally in Belousov-Zhabotinsky solution [7,26].

With the increasing interest in chimera states research, nonidentical oscillator systems have become a focus of attention due to their proximity to actual systems. Laing conducted a study on a ring of nonidentical phase oscillators with natural frequencies following a Lorentz distribution whose width measures the frequency heterogeneity [38]. Theoretical analysis and numerical simulations revealed that strong frequency heterogeneity (large width) may destroy chimera states. However, Dai *et al.* reported that chimera states can exist in a ring of nonlocally coupled bicomponent phase oscillators regardless of the strength of frequency heterogeneity [39]. In their work, the natural frequency distribution was modeled by a double-delta-function distribution, some oscillators with natural frequency ω_0 and others with $-\omega_0$. By treating the two groups of oscillators separately, they found that weak frequency heterogeneity supports two synchronous chimera states while strong frequency heterogeneity supports two asynchronous chimera states. Similar results were also obtained by Zhang *et al.* in a ring of nonlocally coupled bicomponent FHN oscillators [40].

Up to now, the studies of chimera dynamics in nonlocally coupled bicomponent oscillators have been carried out only in one-dimensional rings. It is of interest to explore whether asynchronous spiral wave chimeras exist in two-dimensional systems under strong heterogeneity and how the spiral wave

*qldai@bupt.edu.cn

chimera dynamics transform between synchronous and asynchronous states. In addition, previous studies have shown that two coexisting spiral waves are separated in space [41]. Their wave arms encounter and collide during propagation. Two spiral waves compete with each other through the interface and the faster spiral wave always takes over the slower one and finally entrains the whole space [42], whereas two spiral waves coexisting at the same territory in space have not yet been observed.

In this paper, we set up the phase oscillator model and the FHN model, respectively, to study a two-dimensional square lattice network of nonlocally coupled bicomponent oscillators. We find that spiral wave chimeras in bicomponent oscillators can coexist in the same territory in an entangled way. The wave arms will pass through each other instead of colliding when they encounter. We also find synchronous spiral wave chimeras at weak heterogeneity and asynchronous spiral wave chimeras at strong heterogeneity. Then, the transition from synchronous to asynchronous states is observed when heterogeneity increases.

The rest of the paper is organized as follows. In Sec. II, the two models are introduced in detail. In Sec. III, we present the results of rich dynamics with different heterogeneity and the transitions between them. Finally, a summary is presented in Sec. IV.

II. MODELS

A. Phase oscillator model

We consider a nonlocally coupled system of phase oscillators located on a square lattice of size $N \times N$. The dynamical equation of the phase oscillators is given by

$$\dot{\theta}_{i,j}(t) = \omega_{i,j} - \frac{A}{N_R} \times \sum_{(m,n)\in B_{R,ij}} \sin[\theta_{i,j}(t) - \theta_{m,n}(t) + \alpha], \quad (1)$$

where $\theta_{i,j}$ and $\omega_{i,j}$ $(1 \leqslant i, j \leqslant N)$ are the phase and the natural frequency of the oscillator at position (i, j) on the square lattice. α is the phase lag. Each oscillator is coupled with the same coupling strength A to other oscillators in a neighborhood given by

$$B_{R,ij} = \{(m,n) : \max\{i-R,1\} \leqslant m \leqslant \min\{i+R,N\}; \max\{j-R,1\} \leqslant n \leqslant \min\{j+R,N\}\}, \quad (2)$$

where R is the coupling range. The definition (2) of the neighborhood suggests open boundary conditions [43] imposed on the model (1). N_R denotes the number of coupling neighbors and is set to be $N_R = (2R+1)^2 - 1$ for each oscillator. The position-dependent complex order parameter is defined as $Z_{i,j} = \frac{1}{N_R}\sum_{(m,n)\in B_{R,ij}} e^{i\theta_{m,n}}$. The amplitude $|Z_{i,j}|$ ranges from 0 to 1 and a larger $|Z_{i,j}|$ indicates a higher degree of coherence in the vicinity of the oscillator at position (i, j).

Here, we use a tunable parameter ω_0 to adjust the heterogeneity of the natural frequencies of the bicomponent oscillators. Every oscillator is randomly assigned the natural frequency ω_0 with the probability p and $-\omega_0$ with the probability $1-p$. For convenience, we call oscillators with the natural frequency ω_0 positive oscillators and those with $-\omega_0$ negative oscillators. In this double-delta-function frequency distribution, the larger the ω_0, the stronger the heterogeneity of the bicomponent oscillators.

B. FitzHugh-Nagumo model

The FitzHugh-Nagumo (FHN) model in the $N \times N$ square lattice we consider is

$$\begin{aligned}\varepsilon_{i,j}\dot{u}_{i,j} &= u_{i,j} - \frac{1}{3}u_{i,j}^3 - v_{i,j} + \frac{\sigma}{N_R} \times \sum_{(m,n)\in B_{R,ij}} [b_{uu}(u_{m,n} - u_{i,j}) + b_{uv}(v_{m,n} - v_{i,j})],\\ \dot{v}_{i,j} &= u_{i,j} + a + \frac{\sigma}{N_R} \times \sum_{(m,n)\in B_{R,ij}} [b_{vu}(u_{m,n} - u_{i,j}) + b_{vv}(v_{m,n} - v_{i,j})].\end{aligned} \quad (3)$$

Here $\varepsilon_{i,j}$, $u_{i,j}$, and $v_{i,j}$ $(1 \leqslant i, j \leqslant N)$ are the time-scale separation parameter, activator variable, and inhibitor variable of the oscillator located at the position (i, j), respectively. Each oscillator couples to the other oscillators in the neighborhood $B_{R,ij}$ with the same coupling strength σ, where $B_{R,ij}$ is given by Eq. (2). The coupling matrix is

$$\begin{bmatrix} b_{uu} & b_{uv} \\ b_{vu} & b_{vv} \end{bmatrix} = \begin{bmatrix} \cos\varphi & \sin\varphi \\ -\sin\varphi & \cos\varphi \end{bmatrix}, \quad (4)$$

where φ is the coupling phase [16]. The dynamics of an isolated FHN oscillator depends on the parameter a, which is a limit cycle for $|a| < 1$ and an equilibrium otherwise. In this paper, we fix $a = 0.5$ and assume that the heterogeneity between the bicomponent oscillators comes from $\varepsilon_{i,j}$. Every oscillator is assigned ε_1 with the probability p and ε_2 with the probability $1-p$. In the following, we will fix ε_1 and then increase ε_2 to enhance heterogeneity in the FHN system.

III. RESULTS

We study spiral wave chimera dynamics in nonlocally coupled bicomponent oscillators and focus on the effects of heterogeneity on spiral dynamics. For this aim, we numerically simulate Eqs. (1) and (3) using a fourth-order Runge-Kutta algorithm with $\delta t = 0.025$. In the following, we set the system size $N = 101$, the coupling range $R = 10$, and $p = 0.5$. To generate a spiral wave, we prepare the initial conditions $\theta_{i,j} = \arctan[(j-j_0)/(i-i_0)]$ for Eq. (1) and $u_{i,j} = 2\sin\{\arctan[(j-j_0)/(i-i_0)]\}$, $v_{i,j} = 2\cos\{\arctan[(j-j_0)/(i-i_0)]\}$ for Eq. (3), with (i_0, j_0) being the center of the square lattice [8].

A. Phase oscillators

We first consider nonlocally coupled bicomponent phase oscillators. In the following, we set $A = 1$ and $\alpha = 0.15\pi$. The heterogeneity ω_0 is the controlling parameter. For ω_0=0, the model reduces to monocomponent phase oscillators where a single spiral wave chimera can be observed. Once the heterogeneity is switched on ($\omega_0 \neq 0$), positive and negative oscillators distribute randomly in space. Considering that

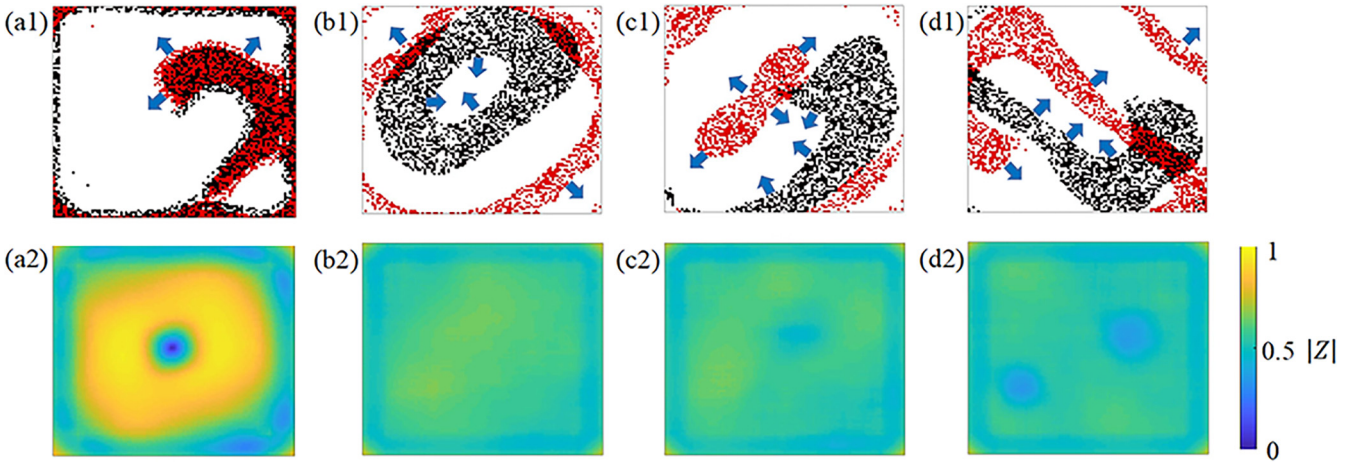

FIG. 1. Different types of dynamical behaviors in nonlocally coupled bicomponent phase oscillators, two synchronous spiral wave chimeras at $\omega_0 = 0.1$ in (a), two target waves at $\omega_0 = 0.9$ in (b), a spiral wave chimera of positive oscillators and a target wave of negative oscillators at $\omega_0 = 1.3$ in (c), and two asynchronous spiral wave chimeras at $\omega_0 = 50$ in (d). The top panels (a1)–(d1) show the snapshots for positive oscillators with $\theta_+ > 1.5\pi$ (black) and negative oscillators with $\theta_- > 1.5\pi$ (red), where the blue arrows indicate the directions of wave propagation. The bottom panels (a2)–(d2) show $|Z|$ (amplitude of position-dependent complex order parameter). The amplitude drops to zero at the centers of incoherent cores, corresponding to the randomized phases. $N = 101$, $R = 10$, $p = 0.5$, $A = 1$, and $\alpha = 0.15\pi$. Animations corresponding to panels (a1)–(d1) are included in the Supplemental Material (Movies 1–4) [44].

the spiral wave chimera in a monocomponent system with positive oscillators has a different rotation frequency from that in a system with negative oscillators, whether spiral wave chimeras can be maintained in bicomponent oscillators becomes an intriguing question. Moreover, if spiral wave chimeras still exist in the presence of heterogeneity, we may further wonder how spiral wave dynamics respond to heterogeneity.

First, spiral wave chimeras do exist in the presence of heterogeneity. Interestingly, the two spiral wave chimeras supported by positive and negative oscillators coexist in the same territory in an entangled way. Especially at weak heterogeneity, the two spiral wave chimeras are synchronized with each other by sharing a same rotating frequency and a same incoherent core. To see it, we take $\omega_0 = 0.1$ as an example and present a snapshot of the phase distribution in space in Fig. 1(a1). To simultaneously visualize the two chimera spiral waves, we binarize the phase of oscillators with a threshold of 1.5π, i.e., oscillators with $\theta_{i,j} \in [0, 1.5\pi]$ are not shown in snapshots. To distinguish the two groups of oscillators, we mark positive oscillators ($\omega_{i,j} = \omega_0$) in black and negative oscillators ($\omega_{i,j} = -\omega_0$) in red. We use θ_+ and θ_- to represent the phase of the positive and negative oscillators, respectively. As shown in Fig. 1(a1) (and Movie 1 in the Supplemental Material [44]), each group of oscillators supports its own spiral wave chimera and the regions of $\theta_+ > 1.5\pi$ and $\theta_- > 1.5\pi$ in the two spiral chimeras almost coincide. The chimera nature of these two spiral waves, characterized by incoherent spiral core, is evidenced in Fig. 1(a2), where the amplitude of the position-dependent complex order parameter, $|Z_{ij}|$, is presented as a heat map. As shown, the spiral region is divided into the coherent wave arm region and the incoherent core region. In the wave arm region, $|Z_{ij}|$ stays close to 1, suggesting the coherent dynamics of oscillators, while in the core region $|Z_{ij}|$ stays close to zero, suggesting the incoherent dynamics of oscillators. Especially, the distribution of $|Z_{ij}|$ in the core region looks like a circular one, which suggests that the two spiral wave chimeras are rigidly rotating ones that share a same incoherent core.

On the other hand, spiral wave chimeras in bicomponent oscillators also exist at strong heterogeneity. Different from weak heterogeneity, the spiral wave chimeras supported by positive and negative oscillators become desynchronized with each other. They do not share the same rotating frequency and the same incoherent core anymore. Figures 1(d1) and 1(d2) show the snapshot of the phases and the amplitudes of the position-dependent complex order parameters at $\omega_0 = 50$ (see Movie 4 in the Supplemental Material [44]). Clearly, both positive and negative oscillators support their own spiral wave chimeras which coexist in the same space in an entangled way. Different from the case with weak heterogeneity, the incoherent cores of the two spiral wave chimeras are distant from each other and, notably, the two spiral chimeras have opposite chirality, with the spiral wave of positive oscillators rotating clockwise and that of negative oscillators rotating counterclockwise. More importantly, by observing the evolution of the two spiral wave chimeras, we find that they rotate at different frequencies, indicating that the coexisting spiral wave chimeras at strong heterogeneity are asynchronous ones.

Now it is interesting to investigate the transition between the synchronous and the asynchronous spiral wave chimeras. As ω_0 increases from 0.1 to 50, three distinct dynamical regimes are identified: the synchronous regime at weak heterogeneity where two spiral wave chimeras are synchronized, the asynchronous regime at strong heterogeneity where the two spiral wave chimeras are asynchronous, and the transition regime roughly in the range of $\omega_0 \in [0.4, 1.3]$. In the transition regime, spiral wave chimeras supported by positive and negative oscillators may yield to target waves. Figure 1(b1) (and Movie 2 in the Supplemental Material [44]) shows an inward propagating target wave of positive oscillators and an outward propagating target wave of negative oscillators at

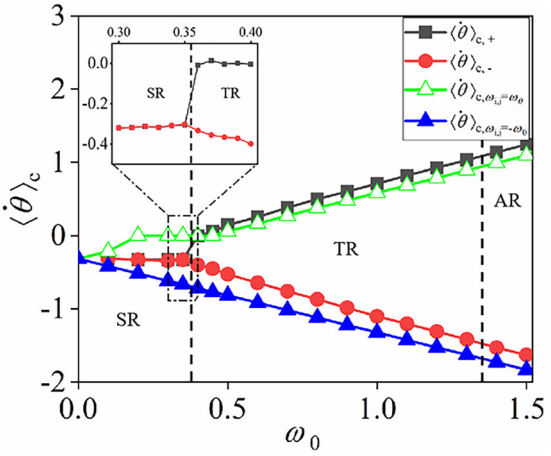

FIG. 2. Mean phase velocities $\langle\dot{\theta}\rangle$ of coherent oscillators of the two groups and monocomponent oscillators are plotted against the heterogeneity parameter ω_0 with $\langle\dot{\theta}\rangle_{c,+}$ represented by black squares, $\langle\dot{\theta}\rangle_{c,-}$ represented by red circles, $\langle\dot{\theta}\rangle_{c,\omega_{i,j}=\omega_0}$ represented by green hollow triangles, and $\langle\dot{\theta}\rangle_{c,\omega_{i,j}=-\omega_0}$ represented by blue solid triangles. Two black dashed lines divide three regimes—the synchronous regime (SR), the transition regime (TR), and the asynchronous regime (AR). The inset shows an enlarged view of $\langle\dot{\theta}\rangle_{c,+}$ and $\langle\dot{\theta}\rangle_{c,-}$ in the dashed box region. $N = 101$, $R = 10$, $p = 0.5$, $A = 1$, and $\alpha = 0.15\pi$.

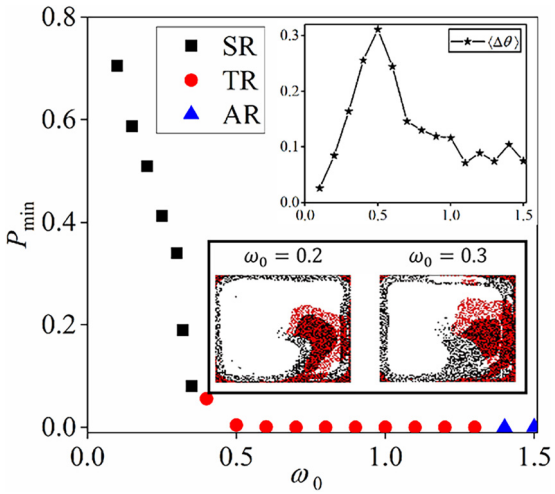

FIG. 3. Minimum proportion $P_{\min}$ of the oscillators in the overlapping area with $\theta_+ > 1.5\pi$ and $\theta_- > 1.5\pi$ to all oscillators with $\theta_\pm > 1.5\pi$ is plotted against ω_0. The black squares, red circles, and blue triangles indicate the results in the synchronous regime (SR), the transition regime (TR), and the asynchronous regime (AR), respectively. The top inset shows the average phase difference $\langle\Delta\theta\rangle$ between positive and negative oscillators with $\theta_+ > 1.5\pi$ and $\theta_- > 1.5\pi$ versus ω_0. The bottom inset shows the snapshots of the phase $\theta_{i,j}$ at $\omega_0 = 0.2$ and $\omega_0 = 0.3$. $N = 101$, $R = 10$, $p = 0.5$, $A = 1$, and $\alpha = 0.15\pi$.

$\omega_0 = 0.9$, where no incoherent area exists [see Fig. 1(b2)]. At $\omega_0 = 1.3$, Figs. 1(c1) and 1(c2) show a spiral wave chimera of positive oscillators together with a target wave of negative oscillators (see Movie 3 in the Supplemental Material [44]). It is worth mentioning that, in our simulations, the combination of spiral wave chimera of negative oscillators and target wave of positive oscillators is never found.

Though the existence of the transition regime interrupts the direct transition from synchronous to asynchronous spiral wave chimeras, we can still investigate the transition between the dynamical behaviors supported by positive and negative oscillators in the sense of synchronization. For this aim, we monitor the mean phase velocities of coherent oscillators in the two groups, denoted by $\langle\dot{\theta}\rangle_{c,\pm}$. Here $\pm$ represents positive and negative oscillators and $\langle\cdot\rangle$ represents the time average over a long time interval. Since coherent oscillators in the same group have the same mean phase velocity which is always lower than those of incoherent ones, we acquire $\langle\dot{\theta}\rangle_{c,\pm}$ by searching for the lowest $\langle\dot{\theta}\rangle_{ij}$ in the two groups [39,40]. Figure 2 shows the results of $\langle\dot{\theta}\rangle_{c,\pm}$ versus the heterogeneity ω_0. As shown in the inset of Fig. 2, the synchronization transition is a discontinuous one where there exists a finite gap between $\langle\dot{\theta}\rangle_{c,\pm}$ at the synchronization transition. On the other hand, Fig. 2 suggests that the transition between the asynchronous and the transition regimes is a continuous one with respect to mean phase velocity. For comparison, we also present the mean phase velocity of the spiral wave chimera in monocomponent oscillators with only positive ones $\langle\dot{\theta}\rangle_{c,\omega_{i,j}=\omega_0}$ or negative ones $\langle\dot{\theta}\rangle_{c,\omega_{i,j}=-\omega_0}$. Clearly, the interaction between positive and negative oscillators slows down the spiral wave chimera of positive oscillators and speeds up that of negative oscillators in the synchronous regime. Actually, the difference between the mean phase velocities of the monocomponent systems with positive and negative oscillators acts as a bifurcation parameter during the synchronization transition, which is similar to the synchronization transition between two coupled nonidentical oscillators.

Then, we investigate the impact of heterogeneity on the synchronous spiral wave chimeras. The bottom inset in Fig. 3 shows the snapshots of the synchronous spiral wave chimeras at $\omega_0 = 0.2$ and $\omega_0 = 0.3$. Together with Fig. 1(a1), we find that the overlap between the regions of $\theta_+ > 1.5\pi$ and $\theta_- > 1.5\pi$ of the two spiral wave chimeras reduces with the increase of ω_0. This suggests that the size of the overlapping region may be treated as a measure on the effective interaction strength between two spiral wave chimeras or, more generally, the interaction strength between the dynamical behaviors of positive and negative oscillators. To be precise, we consider the proportion P of the oscillators within the overlapping region with $\theta_+ > 1.5\pi$ and $\theta_- > 1.5\pi$ (for either spiral waves or target waves) to all oscillators with $\theta_\pm > 1.5\pi$. Typically, P fluctuates with time and, for convenience, we treat the minimum value $P_{\min}$ in the time series of P as such a measure. We present $P_{\min}$ against ω_0 in Fig. 3. As shown, $P_{\min}$ monotonically drops to a low value with the increase of ω_0 in the synchronous regime. In other words, increasing ω_0 decreases the effective interaction strength monotonically. Beyond the synchronization transition, the effective interaction strength becomes so weak that it cannot compensate for the large mismatch of the mean phase velocities of monocomponent systems of positive and negative oscillators, and then desynchronization occurs. Figure 3 also shows that, in the asynchronous regime and most of the transition regime, the effective interaction strength stays at zero. In addition, we

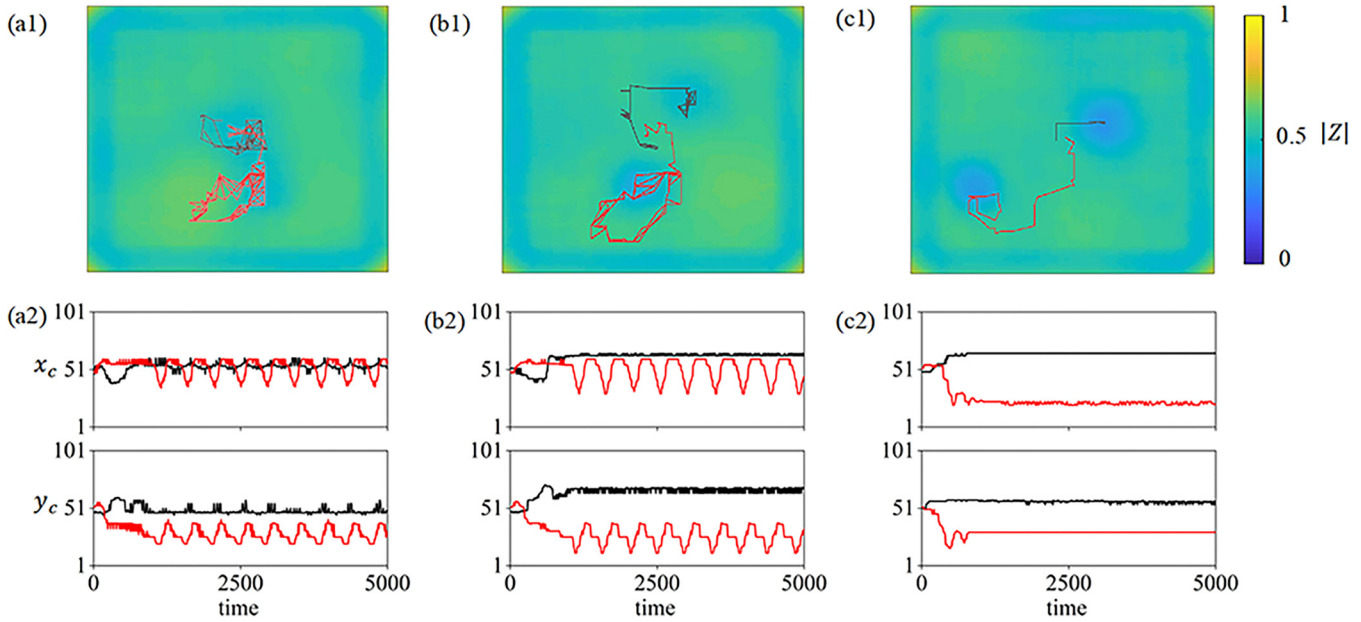

FIG. 4. Trajectories of the incoherent cores of spiral wave chimeras of positive oscillators (black) and negative oscillators (red) at $\omega_0 = 2$ (a), $\omega_0 = 5$ (b), and $\omega_0 = 10$ (c). The top panels (a1)–(c1) show the amplitude distribution of position-dependent complex order parameter $|Z|$ in two-dimensional space. The bottom panels (a2)–(c2) show the position of incoherent cores of positive oscillators (black lines) and negative oscillators (red lines) versus time. x_c and y_c denote the horizontal and vertical coordinates of incoherent cores. $N = 101$, $R = 10$, $p = 0.5$, $A = 1$, and $\alpha = 0.15\pi$.

monitor the average phase difference $\langle \Delta\theta \rangle$ between positive and negative oscillators with $\theta_+ > 1.5\pi$ and $\theta_- > 1.5\pi$ and its dependence on ω_0 is presented in the top inset of Fig. 3. When $\omega_0 \leqslant 0.5$, $\langle \Delta\theta \rangle$ monotonically increases, corresponding to a decreasing degree of synchronization between the two synchronized spiral wave chimeras, which is consistent with the results of $P_{\min}$. When $\omega_0 > 0.5$, the two groups of oscillators become asynchronous, which leads their phases to be irrelevant. Consequently, $\langle \Delta\theta \rangle$ between the two groups decreases with the increase of ω_0.

So far, our results point out that heterogeneity has adverse effects on the synchronous spiral wave chimeras. However, stronger heterogeneity enhances the stability of asynchronous spiral wave chimeras in bicomponent systems. Increasing heterogeneity leads asynchronous spiral wave chimeras from irregularly meandering to rigidly rotating ones. To illustrate it, we track the core trajectories of the two asynchronous spiral wave chimeras. Here, we determine the positions of the two incoherent cores according to the positions of the minimum complex order parameter amplitudes $|Z_{ij}|$ in each group. At $\omega_0 = 2$, the incoherent core of positive oscillators presented in Fig. 4(a1) seems to perform an irregular motion, while the incoherent core of negative oscillators performs a periodic motion, which indicates a periodic meandering spiral wave chimera of negative oscillators. It is further confirmed by the time series of their coordinates in Fig. 4(a2). At $\omega_0 = 5$, the irregular motions of the incoherent cores are suppressed. As shown in Figs. 4(b1) and 4(b2), the location of the incoherent core of positive oscillators is almost unchanged after a transient of meandering, which indicates a rigidly rotating spiral wave chimera, while the incoherent core of negative oscillators still performs a periodic motion. Further increasing heterogeneity to $\omega_0 = 10$, Figs. 4(c1) and 4(c2) show that periodical meandering spiral wave chimera of negative oscillators also yields to a rigidly rotating one. The transition from irregularly meandering spiral wave chimeras to rigidly rotating ones is consistent with the behavior of the effective interaction strength in Fig. 3. To be mentioned, at sufficiently large ω_0, though starting with the almost same location, the two rigidly rotating spiral wave chimeras get to drift away from each other and the distance between their incoherent cores settles down to around $0.5N$.

Actually, spiral wave chimera dynamics in bicomponent phase oscillators can be better illustrated by studying a special case in which, instead of random distribution, positive (negative) oscillators sit on the sites (i, j) with even (odd) $i + j$. With this setup, any two neighboring phase oscillators have different natural frequencies. We divide phase oscillators into four subsets: the subset consisting of oscillators with location $(2i - 1, 2j - 1)$ $[i, j = 1, 2, \ldots, (N + 1)/2]$, the subset with $(2i - 1, 2j)$, the subset with $(2i, 2j - 1)$, and the subset with $(2i, 2j)$. In Fig. 5, we present snapshots of $\theta_{i,j}$ of these four subsets at three different ω_0. Each subset displays a clear pattern and the incoherent cores of spiral waves can be well visualized. Similar to random distribution of positive and negative oscillators, there also exist three dynamic regimes: the synchronous regime at weak heterogeneity (the top panels in Fig. 5), the transition regime at intermediate heterogeneity (the middle panels in Fig. 5), and the asynchronous regime at strong heterogeneity (the bottom panels in Fig. 5). Interestingly, the bottom panels in Fig. 5 show that the two asynchronous spiral wave chimeras at $\omega_0 = 50$ share a same incoherent core, which is a little different from the results in Fig. 1(d).

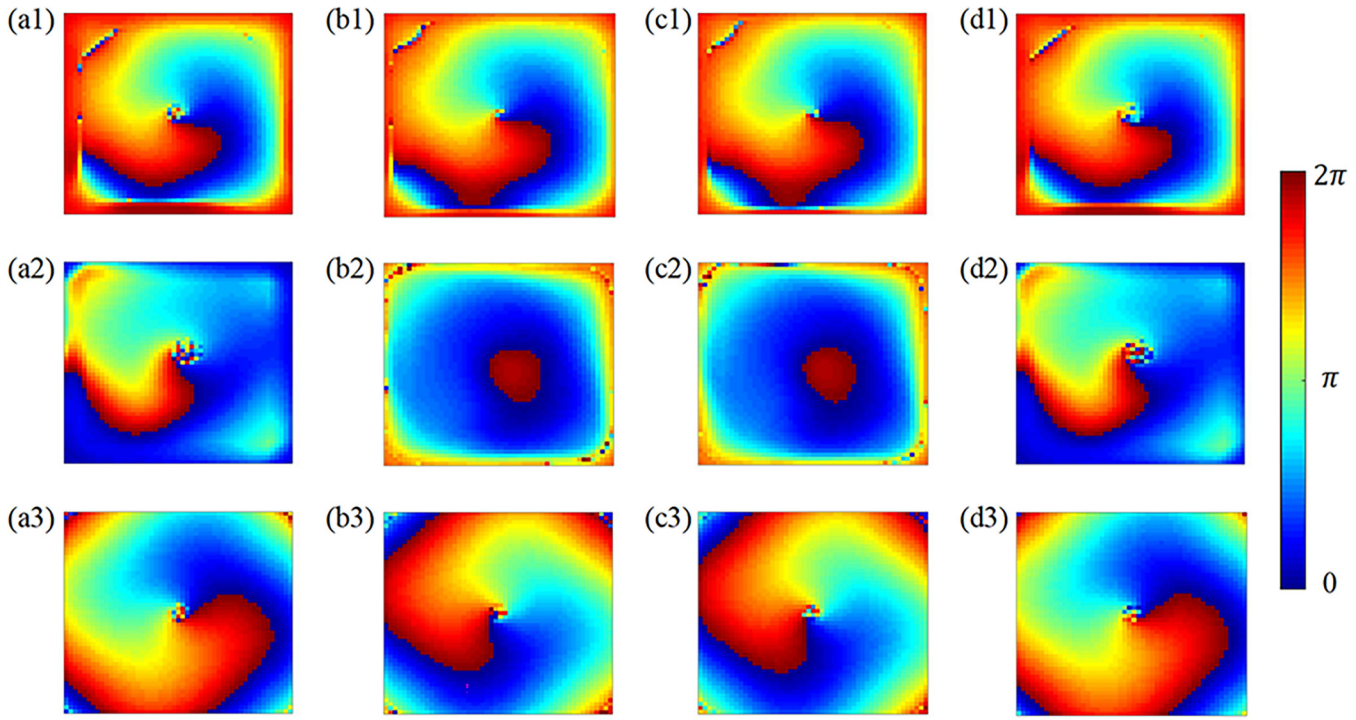

FIG. 5. Top, middle, and bottom panels show the snapshots of the phase $\theta_{i,j}$ of four different subsets at $\omega_0 = 0.1$, $\omega_0 = 0.6$, and $\omega_0 = 50$. Panels (a1)–(a3) for the subset in which oscillators locate at positions with $(2i-1, 2j-1)$. (b1)–(b3) The subset with $(2i-1, 2j)$. (c1)–(c3) The subset with $(2i, 2j-1)$. (d1)–(d3) The subset with $(2i, 2j)$. $N = 101$, $R = 10$, $p = 0.5$, $A = 1$, and $\alpha = 0.15\pi$. Animations are shown in the Supplemental Material (Movies 5–7) [44].

In the continuum limit case, i.e., when $N \to \infty$, the spiral wave chimeras in Eq. (1) can be analyzed using the Ott-Antonsen (OA) ansatz [45]. The square domain is set to be $(x, y) \in [0, 2\pi] \times [0, 2\pi]$. We introduce the probability density function $f_\pm(x, y, \theta, t)$ as the fraction of positive and negative oscillators with phases between θ and $\theta + d\theta$ at time t and position (x, y), respectively. The two functions satisfy the continuity equations

$$\frac{\partial f_\pm}{\partial t} + \frac{\partial (f_\pm v_\pm)}{\partial \theta} = 0, \tag{5}$$

where

$$v_\pm = \dot{\theta}_\pm = \pm\omega_0 - \frac{A}{2i}\left[Z_\pm^* e^{i(\theta+\alpha)} - Z_\pm e^{-i(\theta+\alpha)}\right]. \tag{6}$$

$Z_\pm$ are the spatially dependent complex order parameter of positive and negative oscillators, which are formulated as

$$Z_\pm(x, y, t) = \int_0^{2\pi}\int_0^{2\pi} G(x-x', y-y') \int_0^{2\pi} e^{i\theta} f_\pm d\theta\, dx' dy', \tag{7}$$

with

$$G(x-x', y-y') = \begin{cases} \frac{1}{(4\pi r)^2}, & |x-x'| \leqslant 2\pi r, \\ & |y-y'| \leqslant 2\pi r, \\ 0, & \text{otherwise}, \end{cases} \tag{8}$$

where $r = R/(N-1)$ is the relative coupling range. Using OA ansatz, we write the probability density function as

$$f_\pm(x, y, \theta, t) = \frac{1}{2\pi}\left\{1 + \sum_{n=1}^{\infty}[a_\pm(x, y, t)^n e^{in\theta} + \text{c.c.}]\right\}, \tag{9}$$

where c.c. is the complex conjugate of the previous term. By substituting Eqs. (6) and (9) into Eqs. (5) and (7), we obtain

$$\begin{aligned} \frac{\partial a_\pm(x, y, t)}{\partial t} &= -i(\pm\omega_0)a_\pm(x, y, t) + \frac{A}{2}[Z_\pm(x, y, t)^* e^{i\alpha} \\ &\quad - Z_\pm(x, y, t)e^{-i\alpha} a_\pm(x, y, t)^2], \\ Z_\pm(x, y, t) &= \frac{1}{(4\pi r)^2}\int_{x-2\pi r}^{x+2\pi r}\int_{y-2\pi r}^{y+2\pi r} a_\pm^*(x', y', t)dx'dy'. \end{aligned} \tag{10}$$

To demonstrate the spiral chimera dynamics in the synchronous, transition, and asynchronous regimes, we numerically simulate Eq. (10). As shown by the snapshots of the arguments $\arg(a_\pm)$, $\arg(a_+)$, and $\arg(a_-)$ for several ω_0 in Fig. 6, the dynamics of two synchronous spiral wave chimeras, a spiral wave chimera and a target wave, two target waves, and two asynchronous spiral wave chimeras, are observed, which are qualitatively in agreement with the results in Fig. 1. In addition, to observe the corresponding evolutions, we provide animations in the Supplemental Material (Movies 8–11) [44].

B. FitzHugh-Nagumo oscillators

Next, we consider nonlocally coupled bicomponent FHN oscillators. Similar to phase oscillators, there exist three dynamical regimes—the synchronous regime at weak heterogeneity, the asynchronous regime at strong heterogeneity, and the transition regime in between. Different from phase oscillators, more complicated spatial patterns may appear due to the

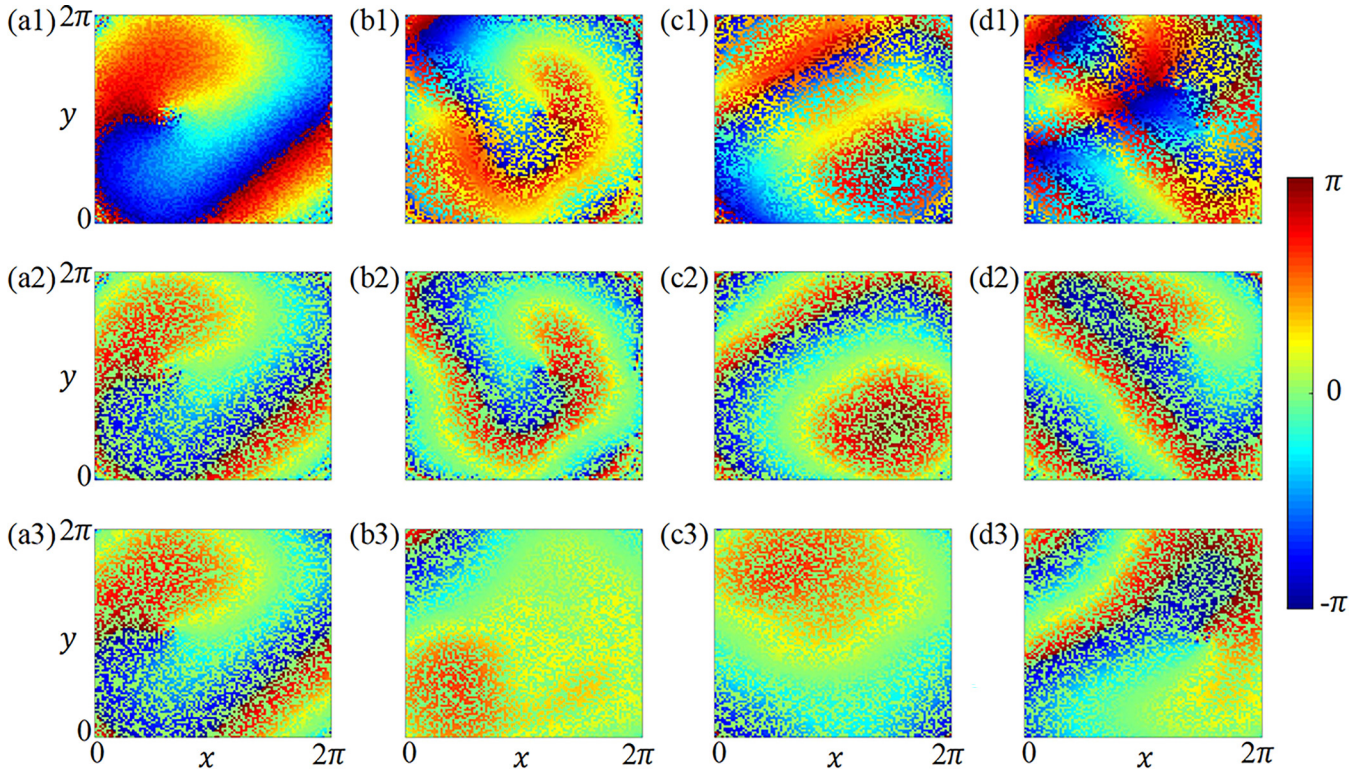

FIG. 6. Top, middle, and bottom panels show the snapshots of the $\arg(a_{\pm})$, $\arg(a_{+})$, and $\arg(a_{-})$ at $\omega_0 = 0.1$ (a), $\omega_0 = 1$ (b), $\omega_0 = 1.5$ (c), and $\omega_0 = 5$ (d). $r = 0.1$, $p = 0.5$, $A = 1$, and $\alpha = 0.15\pi$. Note that, in the middle and bottom panels, the values of $\arg(a_{+})$ for negative oscillators and $\arg(a_{-})$ for positive oscillators are replaced by zero. Animations are shown in the Supplemental Material (Movies 8–11) [44].

rich spatial patterns in nonlocally coupled monocomponent FHN oscillators [35]. More importantly, the transition from synchronous to asynchronous dynamical behaviors also looks like a continuous one in the sense of synchronization. To illustrate these, we set $a = 0.5$, $\sigma = 0.1$, $\varphi = 1.2$, and $\varepsilon_1 = 0.04$. ε_2 is used as a controlling parameter for heterogeneity and varies in the range from 0.04 to 0.5.

In Fig. 7, the snapshots at different ε_2 are presented where the variable u is binarized with the threshold of 1, i.e., oscillators with $u_{i,j} \leqslant 1$ are not shown in snapshots. In the synchronous regime, the spiral wave chimera in ε_1 group is synchronized with the one in ε_2 group. For example, Fig. 7(a) shows synchronous counterclockwise inward propagating double-spiral wave chimeras at $\varepsilon_2 = 0.0405$, while Fig. 7(b) shows synchronous clockwise inward propagating single-spiral wave chimeras. In the transition regime, inward propagating target waves at $\varepsilon_2 = 0.055$ are presented in Fig. 7(c). In the asynchronous regime, complicated dynamics are observed. For example, a clockwise inward propagating single-spiral wave in ε_2 group and a complex pattern in ε_1 group consisting of several spiral wave chimeras at $\varepsilon_2 = 0.07$ in Fig. 7(d), two asynchronous spiral wave chimera pairs (double-spiral waves with wave arms rotating in opposite directions) at $\varepsilon_2 = 0.1$ in Fig. 7(e), and a counterclockwise inward propagating double-spiral wave in ε_1 group and a complex pattern in ε_2 group composed of a spiral wave chimera, a target wave, and a traveling wave at $\varepsilon_2 = 0.5$ in Fig. 7(f). As these dynamics are easier to understand from animations, we refer to the videos in the Supplemental Material (Movies 12–17) [44].

The transition from synchronous to asynchronous dynamics in the bicomponent FHN model can be investigated by monitoring the mean phase velocity Ω_c of coherent oscillators in ε_1 and ε_2 groups calculated as $\Omega_c = 2\pi M_c/\Delta T$, where M_c represents the number of periods of each coherent oscillator during a sufficiently long time interval ΔT. Figure 8(a) plots Ω_c against ε_2. As shown, the coherent oscillators in ε_1 and ε_2 groups share the same mean phase velocity in the synchronous regime, while the mean phase velocities of the coherent oscillators in ε_1 and ε_2 groups get large discrepancy in the asynchronous regime. For comparison, we also present the mean phase velocity of the spiral wave chimera in monocomponent oscillators with $\varepsilon_{i,j} = \varepsilon_2$. Different from phase oscillators, the inset of Fig. 8(a) shows that the synchronization transition is a continuous one where the discrepancy of the mean phase velocities between the two groups increases gradually from zero with the increase of ε_2. Furthermore, we consider the impact of heterogeneity on the synchronous spiral wave chimeras. The proportion of oscillators in the overlapping region of $u_{\varepsilon_1} > 1$ and $u_{\varepsilon_2} > 1$ is monitored and the minimum of P, $P_{\min}$, in the evolution is used to measure the effective interaction strength between ε_1 and ε_2 groups. As shown in Fig. 8(b), the overlapping area between ε_1 and ε_2 groups decreases quickly with the increase of ε_2 in the synchronous regime and $P_{\min}$ remains zero in the asynchronous regime, which is similar to those for phase oscillators.

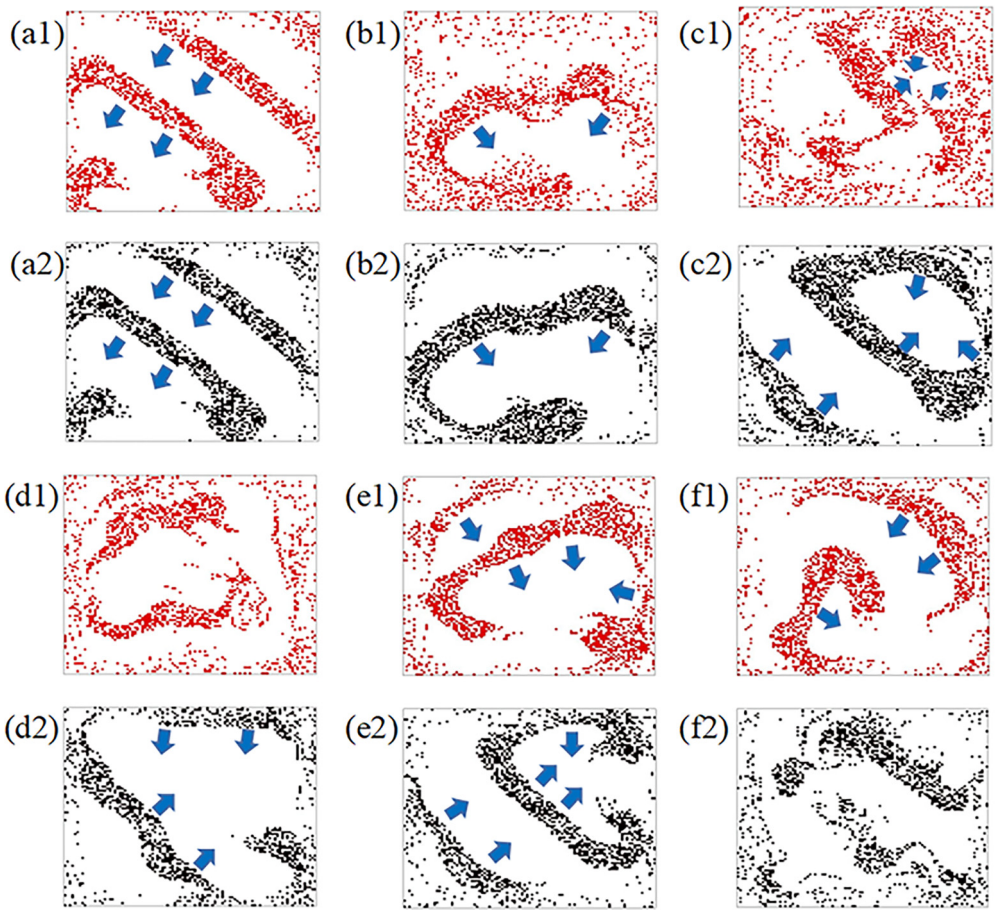

FIG. 7. Different types of dynamical behaviors in nonlocally coupled bicomponent FHN oscillators at different heterogeneities. The snapshots of the activator variable u at $\varepsilon_2 = 0.0405$ (a), $\varepsilon_2 = 0.05$ (b), $\varepsilon_2 = 0.055$ (c), $\varepsilon_2 = 0.07$ (d), $\varepsilon_2 = 0.1$ (e), and $\varepsilon_2 = 0.5$ (f). Panels (a1)–(f1) show the snapshots for ε_1 group oscillators with $u_{\varepsilon_1} > 1$ (red) and (a2)–(f2) show the snapshots for ε_2 group oscillators with $u_{\varepsilon_2} > 1$ (black). Blue arrows indicate the directions of wave propagation. $N = 101$, $R = 10$, $p = 0.5$, $a = 0.5$, $\sigma = 0.1$, and $\varphi = 1.2$. Animations corresponding to panels (a)–(f) are included in the Supplemental Material (Movies 12–17) [44].

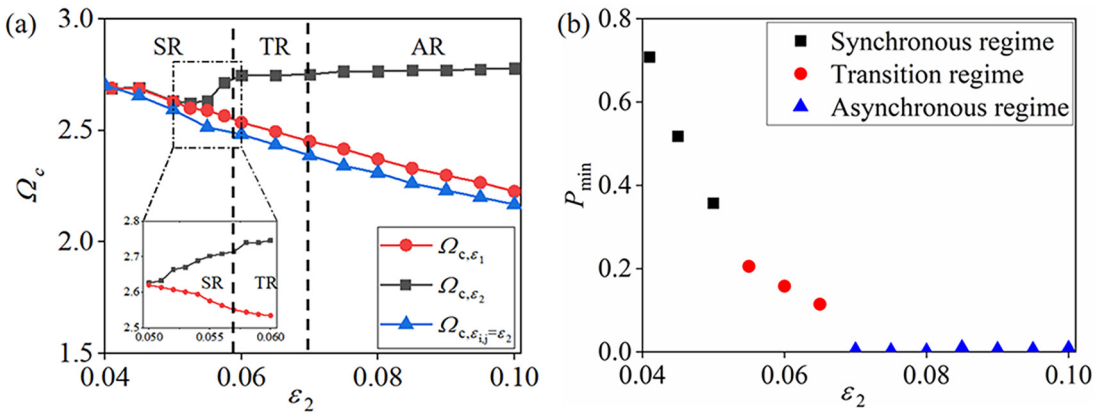

FIG. 8. (a) Mean phase velocities of coherent oscillators in ε_1 group Ω_{c,ε_1} (red circles), ε_2 group Ω_{c,ε_2} (black squares), and monocomponent oscillators $\Omega_{c,\varepsilon_{i,j}=\varepsilon_2}$ (blue triangles) are plotted against the heterogeneity parameter ε_2. Two black dashed lines divide three regimes—the synchronous regime (SR), the transition regime (TR), and the asynchronous regime (AR). The inset shows an enlarged view of Ω_{c,ε_1} and Ω_{c,ε_2} in the dashed box region. (b) The minimum proportion $P_{\min}$ of the oscillators in the overlapping area with $u_{\varepsilon_1} > 1$ and $u_{\varepsilon_2} > 1$ to all oscillators is plotted against ε_2. The black squares, red circles, and blue triangles indicate the results in the synchronous regime, the transition regime, and the asynchronous regime, respectively. $N = 101$, $R = 10$, $p = 0.5$, $a = 0.5$, $\sigma = 0.1$, and $\varphi = 1.2$.

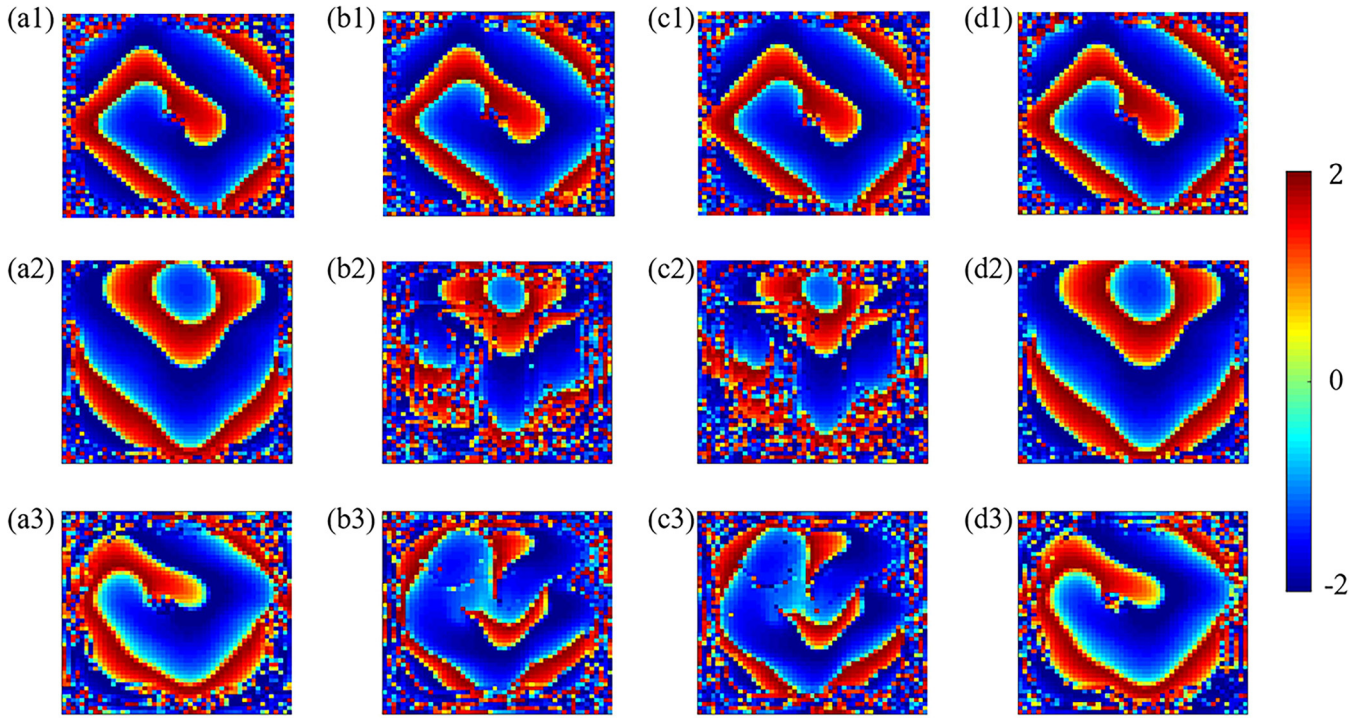

FIG. 9. Top, middle, and bottom panels show the snapshots of the $u_{i,j}$ of four different subsets at $\varepsilon_2 = 0.0405$, $\varepsilon_2 = 0.05$, and $\varepsilon_2 = 0.1$. Panels (a1)–(a3) for the subset in which oscillators locate at positions with $(2i-1, 2j-1)$. (b1)–(b3) The subset with $(2i-1, 2j)$. (c1)–(c3) The subset with $(2i, 2j-1)$. (d1)–(d3) The subset with $(2i, 2j)$. $N = 101$, $R = 10$, $p = 0.5$, $a = 0.5$, $\sigma = 0.1$, and $\varphi = 1.2$. Animations are shown in the Supplemental Material (Movies 18–20) [44].

A nonrandom distribution of the two groups is also studied for FHN oscillators, in which oscillators sitting on the sites (i, j) with even (odd) $i + j$ are assigned with ε_2 (ε_1). As shown in Fig. 9, the snapshots of $u_{i,j}$ of four subsets of FHN oscillators at three different ε_2 demonstrate the dynamics of the synchronous regime, the transition regime, and the asynchronous regime, respectively.

IV. CONCLUSIONS

In conclusion, we have considered nonlocally coupled bicomponent oscillators in a square lattice with open boundaries and investigated the effects of heterogeneity on spiral wave chimeras. The phase oscillators and the FHN oscillators are used as examples since they are two paradigmatic models in nonlinear dynamics. The natural frequency of phase oscillators and the time-scale separation parameter of FHN oscillators are chosen as the heterogeneity parameters, respectively. We find that each group of oscillators supports its own spiral wave chimera and two spiral wave chimeras coexist with each other for both models. There exist three dynamic regimes: the synchronous regime at weak heterogeneity where spiral wave chimeras of the two groups are synchronized with each other, the transition regime at intermediate heterogeneity where spiral wave chimera may yield to target waves, and the asynchronous regime at strong heterogeneity where spiral wave chimeras of the two groups are asynchronous. The existence of these three dynamic regimes is also confirmed by the simulating results of a nonrandom distribution of the two group oscillators and the theoretical analysis based on the OA ansatz in the infinite number of phase oscillators. The synchronization transition from synchronous to asynchronous spiral wave chimeras has been investigated. We find that the transition is a discontinuous one for phase oscillators and a continuous one for the FHN oscillators. We also find that increasing heterogeneity leads to the transition from an irregularly meandering spiral wave chimera to a rigidly rotating one for the phase oscillators.

[1] Y. Kuramoto and D. Battogtokh, Nonlinear Phenom. Complex Syst. **5**, 380 (2002).
[2] D. M. Abrams and S. H. Strogatz, Phys. Rev. Lett. **93**, 174102 (2004).
[3] D. M. Abrams, R. Mirollo, S. H. Strogatz, and D. A. Wiley, Phys. Rev. Lett. **101**, 084103 (2008).
[4] Y. Zhang and A. E. Motter, Phys. Rev. Lett. **126**, 094101 (2021).
[5] A. Ragavan, M. Manoranjani, D. V. Senthilkumar, and V. K. Chandrasekar, Phys. Rev. E **107**, 044209 (2023).
[6] V. O. Munyayev, M. I. Bolotov, L. A. Smirnov, G. V. Osipov, and I. Belykh, Phys. Rev. Lett. **130**, 107201 (2023).
[7] M. R. Tinsley, S. Nkomo, and K. Showalter, Nat. Phys. **8**, 662 (2012).
[8] J. F. Totz, J. Rode, M. R. Tinsley, K. Showalter, and H. Engel, Nat. Phys. **14**, 282 (2018).

[9] S. S. Gavrilov, Phys. Rev. Lett. **120**, 033901 (2018).
[10] N. Lazarides, G. Neofotistos, and G. P. Tsironis, Phys. Rev. B **91**, 054303 (2015).
[11] T. Kapitaniak, P. Kuzma, J. Wojewoda, K. Czolczynski, and Y. Maistrenko, Sci. Rep. **4**, 6379 (2014).
[12] S. Olmi, E. A. Martens, S. Thutupalli, and A. Torcini, Phys. Rev. E **92**, 030901(R) (2015).
[13] L. Schülen, A. Gerdes, M. Wolfrum, and A. Zakharova, Phys. Rev. E **106**, L042203 (2022).
[14] B. Chakrabarti, M. J. Shelley, and S. Fürthauer, Phys. Rev. Lett. **130**, 128202 (2023).
[15] I. Omelchenko, Y. Maistrenko, P. Hövel, and E. Schöll, Phys. Rev. Lett. **106**, 234102 (2011).
[16] I. Omelchenko, O. E. Omel'chenko, P. Hövel, and E. Schöll, Phys. Rev. Lett. **110**, 224101 (2013).
[17] O. E. Omel'chenko, Y. L. Maistrenko, and P. A. Tass, Phys. Rev. Lett. **100**, 044105 (2008).
[18] G. C. Sethia and A. Sen, Phys. Rev. Lett. **112**, 144101 (2014).
[19] A. Zakharova, M. Kapeller, and E. Schöll, Phys. Rev. Lett. **112**, 154101 (2014).
[20] A. Yeldesbay, A. Pikovsky, and M. Rosenblum, Phys. Rev. Lett. **112**, 144103 (2014).
[21] I. Omelchenko, A. Zakharova, P. Hövel, J. Siebert, and E. Schöll, Chaos **25**, 083104 (2015).
[22] J. Hizanidis, V. G. Kanas, A. Bezerianos, and T. Bountis, Int. J. Bifurcat. Chaos **24**, 1450030 (2014).
[23] B. K. Bera, D. Ghosh, and M. Lakshmanan, Phys. Rev. E **93**, 012205 (2016).
[24] C. R. Hens, A. Mishra, P. K. Roy, A. Sen, and S. K. Dana, Pramana-J. Phys. **84**, 229 (2015).
[25] A. M. Hagerstrom, T. E. Murphy, R. Roy, P. Hövel, I. Omelchenko, and E. Schöll, Nat. Phys. **8**, 658 (2012).
[26] S. Nkomo, M. R. Tinsley, and K. Showalter, Phys. Rev. Lett. **110**, 244102 (2013).
[27] E. A. Martens, S. Thutupalli, A. Fourrière, and O. Hallatschek, Proc. Natl. Acad. Sci. USA **110**, 10563 (2013).
[28] N. C. Rattenborg, C. J. Amlaner, and S. L. Lima, Neurosci. Biobehav. Rev. **24**, 817 (2000).
[29] S.-I. Shima and Y. Kuramoto, Phys. Rev. E **69**, 036213 (2004).
[30] O. E. Omel'chenko, M. Wolfrum, S. Yanchuk, Y. L. Maistrenko, and O. Sudakov, Phys. Rev. E **85**, 036210 (2012).
[31] M. J. Panaggio and D. M. Abrams, Phys. Rev. Lett. **110**, 094102 (2013).
[32] M. J. Panaggio and D. M. Abrams, Phys. Rev. E **91**, 022909 (2015).
[33] E. A. Martens, C. R. Laing, and S. H. Strogatz, Phys. Rev. Lett. **104**, 044101 (2010).
[34] M. Bataille-Gonzalez, M. G. Clerc, and O. E. Omel'chenko, Phys. Rev. E **104**, L022203 (2021).
[35] S. Guo, Q. Dai, H. Cheng, H. Li, F. Xie, and J. Yang, Chaos, Solitons Fractals **114**, 394 (2018).
[36] A. Schmidt, T. Kasimatis, J. Hizanidis, A. Provata, and P. Hövel, Phys. Rev. E **95**, 032224 (2017).
[37] C. Gu, G. St-Yves, and J. Davidsen, Phys. Rev. Lett. **111**, 134101 (2013).
[38] C. R. Laing, Physica D **238**, 1569 (2009).
[39] Q.-L. Dai, X.-X. Liu, K. Yang, H.-Y. Cheng, H.-H. Li, F. Xie, and J.-Z. Yang, Front. Phys. **15**, 62501 (2020).
[40] Y. Zhang, P. Wang, M. Zhang, and J. Yang, Europhys. Lett. **135**, 40004 (2021).
[41] A. T. Winfree, Physica D **49**, 125 (1991).
[42] Z. Cao, P. Li, H. Zhang, F. Xie, and G. Hu, Chaos **17**, 015107 (2007).
[43] T. E. Lee and M. C. Cross, Phys. Rev. Lett. **106**, 143001 (2011).
[44] See Supplemental Material at http://link.aps.org/supplemental/10.1103/PhysRevE.108.064206 for animations that complement Figs. 1(a1)–1(d1), 5–7, and 9.
[45] E. Ott and T. M. Antonsen, Chaos **18**, 037113 (2008).